

Effective mass in mixed-dimensionality pseudo-Proca systems, g -factor corrections, and the radiative effects to the interaction potential

Rodrigo F. Ozela^{1,2,*} Van Sérgio Alves^{1,†} Leandro O. Nascimento^{1,3,‡} E. C. Marino^{4,§}
C. Morais Smith^{2,||} R. O. Ramos^{5,¶} and J. F. Medeiros Neto^{1,**}

¹*Faculdade de Física, Universidade Federal do Pará, 66075-110 Belém, PA, Brazil*

²*Utrecht University, Institute for Theoretical Physics, 3584 CC Utrecht, Netherlands*

³*Universidade Federal de Campina Grande, Avenida Aprígio Veloso 882, 58429-900, Campina Grande, Paraíba, Brazil*

⁴*Instituto de Física, Universidade Federal do Rio de Janeiro, 21941-972, Rio de Janeiro, RJ, Brazil*

⁵*Departamento de Física Teórica, Universidade do Estado do Rio de Janeiro, 20550-013 Rio de Janeiro, RJ, Brazil*



(Received 5 May 2023; accepted 22 May 2023; published 20 September 2023)

In this work, we study a model that describes the $(2 + 1)$ D Yukawa interaction for static particles confined to the plane. In order to do so, we perform a dimensional reduction of a $(3 + 1)$ D massive vector field whose mass term introduces a natural scale for a correlation length within the system. We derive the projected model similarly to the so-called pseudo (or reduced) quantum electrodynamics that has been used in several applications. One-loop radiative corrections to the electron and to the massive vector-field mass are computed, as well as the vertex corrections; this brings forth the quantum correction to the electron g factor, demonstrating that it smoothly goes to zero when the mass of the vector field is significantly larger than the electron mass and generalizing the results obtained for graphene within pseudo-QED to a system with a correlation length. Such a limit is expected to emerge due to many-body interactions in two-dimensional materials. Furthermore, the model is likely to be relevant in the relativistic limit, when electrons move with a high velocity.

DOI: [10.1103/PhysRevD.108.056017](https://doi.org/10.1103/PhysRevD.108.056017)

I. INTRODUCTION

The use of quantum field theories (QFT) to describe two-dimensional systems has gained increased attention during the past years. This is due to the great agreement obtained between the theoretical predictions and the experimental data in many condensed-matter systems. Examples range from the integer and the fractional quantum Hall effects [1–5] to the study of transport in graphene [6–14], excitonic properties of transition metal dichalcogenides (TMDs) [15–17], and superconductivity in layered materials [18–22].

The quantum field description of the electron-electron interactions in planar systems is rather involved, because the system has mixed dimensionality: The field mediating the interactions lives in $(3 + 1)$ D, whereas the electron kinematics is constrained to a two-dimensional spatial

plane [see Fig. 1(a)]. The appropriate theory to capture this dimensional mismatch is the so-called pseudo-quantum electrodynamics (PQED) [23] (sometimes also referred to as reduced QED [24–26]). In this approach, a planar field emulates the properties of the $(3 + 1)$ D electromagnetic field, acting as an effective projection [see Fig. 1(b)].

The PQED has been demonstrated to be unitary [27] and causal [28] and has been successfully applied to describe several properties of very thin systems (graphene-like structures) [13,29], where the $2d$ approximation is a reasonable assumption. We highlight the Fermi velocity renormalization in the absence [12] or in the presence [14] of a magnetic field, in the vicinity of a grounded conducting surface [30], or in a cavity [31]. In addition, it provided a theoretical description of the quantum valley Hall effect, quantum corrections for the longitudinal conductivity in graphene [13], and the corrections to the electron's g factor due to interactions [32]. When accounting for massive electrons, the theory was shown to describe the excitonic spectrum [16] and the renormalization of the band gap in TMDs [29] and dynamical chiral symmetry breaking [33]. A dual PQED type of model describing the interaction between point vortex excitations and with some interesting properties has also been recently constructed [34].

*ozelarf@gmail.com

†vansergi@ufpa.br

‡lon@ufpa.br

§marino@if.ufrj.br

||c.demoraissmith@uu.nl

¶rudnei@uerj.br

**jfmn@ufpa.br

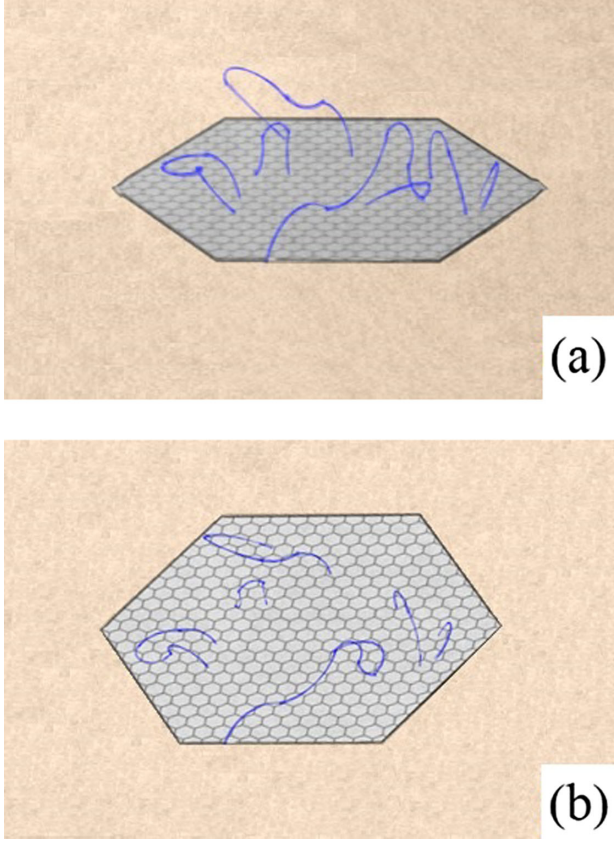


FIG. 1. Schematic representation of a mixed-dimensionality system. In (a), the hexagonal plate is the part of the system which is constrained to a plane, while the blue lines picture any arbitrary-interaction mediator that can detach from the plane as long as it returns to the plane. In (b), the blue lines lie within the hexagonal plane and are the effective projection of the lines in (a).

Another topic that attracted much attention recently is the study of models with broken Lorentz symmetry within massive-photon theories [35]. This is often investigated in the context of nonrenormalizable effective field theories [36–38] or in the lookout for valid quantum gravity frameworks [39,40]. All these models, however, lacked the projection component to describe the aforementioned mixed-dimensionality effect, which are accounted for within the PQED.

Here, we will follow steps similar to the ones that led to the construction of the PQED model [23] and develop a theory to describe electron-electron interactions through a *massive* vector (Proca) field in a (soft) broken Lorentz symmetry context. For a discussion about the projection of the Proca model, see Ref. [41], which shows that a Yukawa potential is generated in the static limit and indicates the relevance of the order in which we generate mass and do the projection. Such a model constrains only the matter (electron) current to the spatial xy plane. The corresponding quantum partition functional is defined initially in $3 + 1$

dimensions, and then the third spatial dimension is integrated out. This procedure is very much analogous to the one that links the $(3 + 1)$ D Maxwell model to the $2 + 1$ -dimensional PQED model.

This work is organized as follows. In Sec. II, we present the model used in this work, and we derive its planar dimensional reduction in a procedure analogous to that used to derive the PQED model. In Sec. III, we compute the electron and the massive vector-field self-energies for the model, as well as the interaction vertex, within the leading-order (one-loop) level. In this same section, we also explicitly derive the g factor for our model. A comparison to the literature, when considering the massless regime, is also established. In Sec. IV, we present our conclusions. Some technical details of the calculation of the g factor are given in the Appendix.

II. PSEUDO-PROCA MODEL

Let us first consider the $(3 + 1)$ D Proca (P) model, including the coupling to a general conserved current J^μ . The quantum partition functional is

$$Z_P[J^\mu] = \int \mathcal{D}A_\mu \exp(iS_P), \quad (2.1)$$

where A_μ is a $(3 + 1)$ D massive vector field and S_P is the action, given by

$$S_P = \int d^4\chi \left(-\frac{1}{4} F_{\mu\nu} F^{\mu\nu} + \frac{m^2}{2} A^\mu A_\mu - e A_\mu J^\mu \right), \quad (2.2)$$

where $F_{\mu\nu} = \partial_\mu A_\nu - \partial_\nu A_\mu$ and m is the vector-field mass. Natural units ($\hbar = c = 1$) are considered for the remainder of this section. The vector-field propagator is directly derived from Eq. (2.2):

$$G_P^{\mu\nu}(\chi - \chi') = \int \frac{d^4k}{(2\pi)^4} \frac{e^{-ik \cdot (\chi - \chi')}}{k^2 - m^2} \left[\eta^{\mu\nu} - \frac{k^\mu k^\nu}{m^2} \right], \quad (2.3)$$

with χ and χ' representing points in the $(3 + 1)$ D spacetime and $\eta^{\mu\nu} = \text{diag}(+, -, -, -)$ is the metric tensor. Integrating out the vector field in Eq. (2.1), we obtain

$$Z_P[J^\mu] = \mathcal{Z}_0 e^{-\frac{1}{2} e^2 \int d^4\chi d^4\chi' J_\mu(\chi) G_P^{\mu\nu}(\chi - \chi') J_\nu(\chi')}, \quad (2.4)$$

where \mathcal{Z}_0 is a normalization constant, independent of J^μ . Note that, by the conservation of the current, $\partial_\mu J^\mu = 0$, the last term in Eq. (2.3) ($k^\mu k^\nu / m^2$) vanishes in Eq. (2.4).

By using the constraint of having only currents in the xy plane, we can explicitly write the current J^μ as

$$J^\mu(\chi) = \begin{cases} \mathcal{J}^\mu(t, x, y) \delta(z), & \text{if } \mu = 0, 1, 2, \\ 0, & \text{if } \mu = 3, \end{cases} \quad (2.5)$$

where the hat over an index notation is used to identify objects that assume three values, i.e., $\hat{\mu} = 0, 1, 2$.

After the integration in z and z' space coordinates, Eq. (2.4) can be written as

$$\mathcal{Z}_{\text{PP}}[\mathcal{J}] = \mathcal{Z}_0 e^{-i\frac{z^2}{2}} \int d^3\zeta d^3\zeta' J_{\hat{\mu}}(\zeta) \mathcal{G}_{\text{P}}^{\hat{\mu}\hat{\nu}}(\zeta - \zeta') J_{\hat{\nu}}(\zeta'), \quad (2.6)$$

with ζ and ζ' denoting points in the $2 + 1$ -dimensional spacetime and $\mathcal{G}_{\text{P}}^{\hat{\mu}\hat{\nu}}(\zeta - \zeta')$ is given by

$$\mathcal{G}_{\text{P}}^{\hat{\mu}\hat{\nu}}(\zeta - \zeta') = i \int \frac{d^4k}{(2\pi)^4} \frac{\eta^{\hat{\mu}\hat{\nu}}}{k^2 - m^2} e^{-ik \cdot (\zeta - \zeta')} \Big|_{z=z'=0}, \quad (2.7)$$

where the momentum integration is over the energy-momentum four-vector k^μ .

If we now perform the integration over the third component of k^μ , i.e., k_z , in Eq. (2.7) and, hence, restrict the dynamics to the xy -space plane, we obtain

$$\mathcal{G}_{\text{P}}^{\hat{\mu}\hat{\nu}}(\zeta - \zeta') = \frac{i}{2} \int \frac{d^3k}{(2\pi)^3} \frac{\eta^{\hat{\mu}\hat{\nu}} e^{-ik \cdot (\zeta - \zeta')}}{\sqrt{k^2 - m^2}}, \quad (2.8)$$

with k now indicating a three-vector, stressing the fact that we are now working in the reduced space (effectively, in $2 + 1$ dimensions). However, the above result can also be obtained if we start from a completely $2 + 1$ -dimensional, in principle nonlocal, model from the very beginning. We will name this model the ‘‘pseudo-Proca’’ (PP) model, in analogy with the case of the PQED model. Notice that the denominator of the propagator in Eq. (2.8) is significantly different from the original Proca model, and this impacts directly the quantum corrections in a mixed-dimensionality physical system.

The Lagrangian density for this model is then expressed as

$$\mathcal{L}_{\text{PP}} = -\frac{1}{2} \frac{F_{\hat{\mu}\hat{\nu}} F^{\hat{\mu}\hat{\nu}}}{\sqrt{-\square - m^2}} - e A_{\hat{\mu}} \mathcal{J}^{\hat{\mu}} - \frac{m^2}{2} \frac{A^{\hat{\mu}} A_{\hat{\mu}}}{\sqrt{-\square - m^2}}, \quad (2.9)$$

with $\mathcal{J}^{\hat{\mu}}$ being the general $2 + 1$ -dimensional current defined in Eq. (2.5) and \square the d'Alembertian operator (which must be understood as a convolution). The free propagator associated with \mathcal{L}_{PP} is simply given by Eq. (2.8), as can be easily verified. Thus, we immediately realize that

$$\mathcal{G}_{\text{PP}}^{\hat{\mu}\hat{\nu}}(\zeta - \zeta') = G_{\text{P}}^{\hat{\mu}\hat{\nu}}(\chi - \chi') \Big|_{z=z'=0}, \quad (2.10)$$

and, therefore, the quantum partition function of the pseudo-Proca and that of the $(3 + 1)$ D Proca models are completely equivalent, as long as the currents of the latter are constrained to a plane, such as in Eq. (2.5). It is important to emphasize that the process we implemented in this section is sensible to the relative order of generating

mass and making the dimensional projection [41], and we chose to first include the Proca term and just then project it.

III. RADIATIVE CORRECTIONS

In this section, we consider a soft symmetry-breaking term in the Dirac action through the Fermi velocity v_F , in order to reproduce the Dirac-like low-energy electronic dispersion. The Lagrangian density in the now $2 + 1$ -dimensional Minkowski space is then

$$\begin{aligned} \mathcal{L} = & -\frac{1}{2} \frac{F_{\mu\nu} F^{\mu\nu}}{\sqrt{-\square - m^2}} - \frac{m^2}{2} \frac{A^\mu A_\mu}{\sqrt{-\square - m^2}} \\ & + \bar{\psi} [i\gamma^0 \partial_0 + i v_F \gamma^i \partial_i - M c^2 - e(\gamma^0 A_0 + \beta \gamma^i A_i)] \psi, \end{aligned} \quad (3.1)$$

with ψ a four-component Dirac spinor, $\beta = v_F/c$, and M the Dirac fermion mass. In the above equation and from this point on, we have explicitly retrieved the dimension of the speed of light c (but still keeping $\hbar = 1$ units). For convenience and to avoid overloading the notation, we suppress the hat of the Lorentz index.

The Feynman rules for the model are obtained as usual [42]. The interaction vertex is given by $\Gamma^\alpha = -ie(\gamma^0, \beta\gamma^i)$, the fermion propagator is

$$S_F(p) = i \left(\frac{\gamma^0 p_0 + v_F \gamma^i p_i + M c^2}{p_0^2 - v_F^2 \mathbf{p}^2 - M^2 c^4} \right), \quad (3.2)$$

and the massive vector-field propagator reads

$$\Delta_{\mu\nu}(p) = -\frac{ic\eta_{\mu\nu}}{2\sqrt{p_0^2 - c^2 \mathbf{p}^2 - m^2 c^4}}. \quad (3.3)$$

A. Electron self-energy

The electron self-energy at one-loop order is shown in Fig. 2, and its regularized amplitude is given by

$$-i\Sigma(p) = \int \frac{d^D k}{(2\pi)^D} \Gamma^\mu S_F(p - k) \Gamma^\nu \Delta_{\mu\nu}(k), \quad (3.4)$$

where $D = d + 1$. In what follows, all momentum integrations in the loop radiative quantities are computed using standard dimensional regularization procedure [43,44],

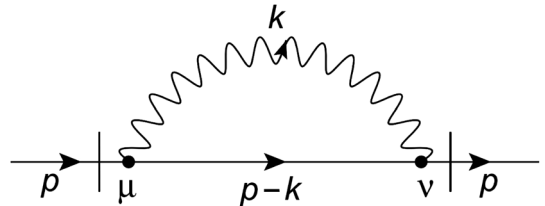


FIG. 2. Feynman diagram for the one-loop correction to the fermion self-energy.

with $e \rightarrow \mu^{\epsilon/2}e$, $d = 2 - \epsilon$, and μ is the dimensional regularization energy scale.

By substituting the propagators and vertices in Eq. (3.4), we obtain

$$-i\Sigma(p) = \frac{(ie)^2 \mu^\epsilon c}{2} \int \frac{d^D k}{(2\pi)^D} \frac{N_1}{D_1}, \quad (3.5)$$

where N_1 and D_1 are given, respectively, by

$$\begin{aligned} N_1 &= v_F(p-k)_i (\gamma^0 \gamma^i \gamma_0 + \beta^2 \gamma^j \gamma^i \gamma_j) + (p-k)_0 \\ &\quad + (\gamma^0 \gamma^0 \gamma_0 + \beta^2 \gamma^j \gamma^0 \gamma_j) + M c^2 (\gamma^0 \gamma_0 + \beta^2 \gamma^j \gamma_j), \\ D_1 &= [(p-k)_0^2 - v_F^2 (\mathbf{p}-\mathbf{k})^2 - M^2 c^4] \\ &\quad \times \sqrt{k_0^2 - c^2 \mathbf{k}^2 - m^2 c^4}. \end{aligned} \quad (3.6)$$

Using, hereinafter, the gamma matrix properties $\gamma^0 \gamma_0 = 1$ and $\gamma^j \gamma_j = 2$, we have that

$$-i\Sigma(p) = \frac{(ie)^2 \mu^\epsilon c}{2} \int \frac{dk_0}{2\pi} \frac{d^d k}{(2\pi)^d} \frac{\gamma^0(p-k)_0(1+2\beta^2) - v_F \gamma^i(p-k)_i + (1+2\beta^2)M c^2}{[(p-k)_0^2 - v_F^2 (\mathbf{p}-\mathbf{k})^2 - M^2 c^4] (\sqrt{k_0^2 - c^2 \mathbf{k}^2 - m^2 c^4})}. \quad (3.7)$$

Using the Feynman parametrization,

$$\frac{1}{a\sqrt{b}} = \frac{3}{4} \int_0^1 dx \left\{ \frac{(1-x)^{-1/2}}{[ax + (1-x)b]^{3/2}} \right\}, \quad (3.8)$$

and performing the integration in k_0 , we obtain that Eq. (3.7) can be rewritten as

$$-i\Sigma(p) = \frac{(ie)^2 \mu^\epsilon c}{4\pi} \int_0^1 \frac{dx}{\sqrt{1-x}} \int \frac{d^d k}{(2\pi)^d} \frac{N_2}{D_2}, \quad (3.9)$$

where N_2 and D_2 are defined, respectively, as

$$\begin{aligned} N_2 &= (1+2\beta^2)M c^2 + (1-2\beta^2)\gamma^0 p_0(1-x) \\ &\quad - \left(1 - \frac{v_F^2 x}{B}\right) v_F \gamma^i p_i, \end{aligned} \quad (3.10)$$

$$D_2 = B \left[\left(\mathbf{k} - \frac{\mathbf{p} v_F^2 x}{B} \right)^2 - \frac{\mathbf{p}^2 v_F^4 x^2}{B^2} + \frac{\mathcal{A}}{B} \right], \quad (3.11)$$

with \mathcal{A} and B defined, respectively, as

$$\begin{aligned} \mathcal{A} &= p_0^2 x^2 + [(M^2 - m^2)c^4 + \mathbf{p}^2 v_F^2 - p_0^2]x + m^2 c^4, \\ B &= c^2 [1 - x(1 - \beta^2)]. \end{aligned} \quad (3.12)$$

The electron self-energy then becomes

$$-i\Sigma(p) = \frac{(ie)^2 c \mu^\epsilon}{4\pi} \int_0^1 \frac{dx}{B \sqrt{1-x}} \int \frac{d^d k}{(2\pi)^d} \frac{N_2}{k^2 - \Delta}, \quad (3.13)$$

$$\Delta = \frac{\mathbf{p}^2 v_F^4 x^2}{B^2} + \frac{\mathcal{A}}{B}. \quad (3.14)$$

Performing the integration in the arbitrary dimension $d = 2 - \epsilon$ in Eq. (3.13) in the dimensional regularization procedure, we obtain

$$\begin{aligned} \Sigma(p) &= \frac{(ie)^2 c \mu^\epsilon}{16\pi^2} \int_0^1 \frac{dx}{\sqrt{1-x}} \frac{\Gamma(\frac{\epsilon}{2}) N_2}{B} \left[\frac{\Delta}{4\pi} \right]^{-\frac{\epsilon}{2}} \\ &= \frac{(ie)^2 c}{16\pi^2} \int_0^1 \frac{dx}{\sqrt{1-x}} \frac{N_2}{B} \left[\frac{2}{\epsilon} - \gamma_E - \ln \left(\frac{\Delta}{4\pi \mu^2} \right) + \mathcal{O}(\epsilon) \right] \\ &= \Sigma_{\text{finite}}(p) + \Sigma_{\text{div}}(p), \end{aligned} \quad (3.15)$$

where

$$\Sigma_{\text{finite}}(p) = -\frac{(ie)^2 c}{16\pi^2} \int_0^1 \frac{dx}{\sqrt{1-x}} \frac{N_2}{B} \left[\gamma_E + \ln \left(\frac{\Delta}{4\pi \mu^2} \right) \right] \quad (3.16)$$

and

$$\Sigma_{\text{div}}(p) = \frac{(ie)^2 c}{8\pi^2 \epsilon} \int_0^1 \frac{dx}{\sqrt{1-x}} \frac{N_2}{B} \quad (3.17)$$

are the finite and divergent contributions to the electron self-energy, respectively, in the pseudo-Proca QED. One notices that the divergent part of the electron self-energy, Eq. (3.17), is independent of the vector-field mass, and it is, in fact, exactly the same result as that obtained in the PQED case [45]. Consequently, the Fermi velocity renormalization will also be the same.

Substituting Eq. (3.10) in Eq. (3.16), we immediately read the one-loop contributions to the electron mass and the wave-function renormalization terms. In particular, the one-loop correction for the fermion mass at zero-external momenta is

$$\begin{aligned} \Sigma_{\text{finite}}^M(0) &= \frac{e^2 c}{16\pi^2} (1+2\beta^2) M \int_0^1 \frac{dx}{\sqrt{1-x}} \frac{1}{1-x(1-\beta^2)} \\ &\quad \times \left\{ \gamma_E + \ln \left[\frac{M^2 c^2 x + m^2 c^2 (1-x)}{4\pi \mu^2 [1-x(1-\beta^2)]} \right] \right\}. \end{aligned} \quad (3.18)$$

The PQED result is obtained by simply setting $m = 0$ in Eq. (3.18).

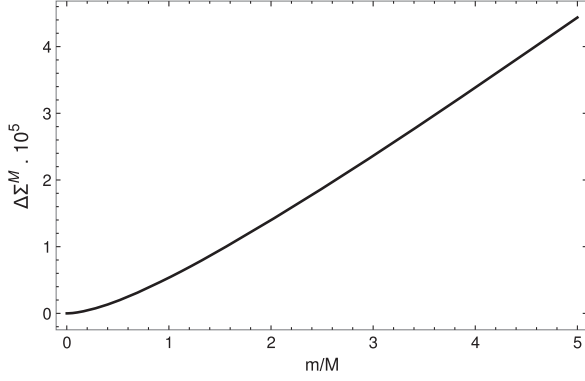


FIG. 3. The difference of the self-energy correction for the fermion mass, with respect to the PQED one, as a function of the mass ratio (m/M). For illustrative purposes only, the Fermi velocity was taken to be $v_F = c/300$, and we also have used $e^2 = 4\pi v_F \alpha$, where $\alpha = 1/137$ is the fine-structure constant.

In Fig. 3, we show the behavior of the ratio $\Delta\Sigma^M \equiv [\Sigma_{\text{finite}}^M(0) - \lim_{m \rightarrow 0} \Sigma_{\text{finite}}^M(0)]/(Mc^2)$ as a function of (m/M). We note that the electron self-energy correction increases with the vector-field mass.

B. The vector-field self-energy

Let us now compute the vector-field self-energy, shown in Fig. 4, for the present model. Explicitly, we have that

$$i\Pi^{\mu\nu}(p_0, \mathbf{p}) = - \int \frac{d^D k}{(2\pi)^D} \text{Tr}[\Gamma^\mu S_F(k+p)\Gamma^\nu S_F(k)]. \quad (3.19)$$

The manipulation of the Dirac algebra proceeds in a standard fashion [42]. Separating the components of the polarization tensor and performing the integration over k_0 and \mathbf{k} in Eq. (3.19), we can write

$$\Pi^{00}(p) = -\frac{e^2}{\pi} \mathbf{p}^2 \Pi(p^2), \quad (3.20)$$

$$\Pi^{ij}(p) = -\frac{e^2}{\pi c^2} [-p^2 \eta^{ij} + v_F^2 p^i p^j] \Pi(p^2), \quad (3.21)$$

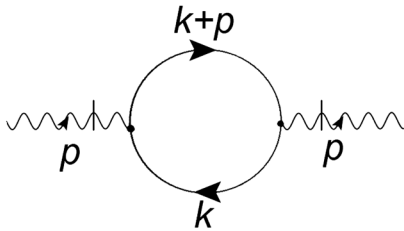


FIG. 4. The one-loop vector-field vacuum polarization diagram.

$$\Pi^{0j}(p) = -\frac{e^2}{\pi c} p^0 p^j \Pi(p^2), \quad (3.22)$$

where $p^2 = p_0^2 - v_F^2 \mathbf{p}^2$ and $\Pi(p^2)$ is given by

$$\Pi(p^2) = \int_0^1 \frac{x(1-x)dx}{\sqrt{M^2 c^4 - p^2 x(1-x)}}. \quad (3.23)$$

Notice that the use of a dimensional regularization scheme makes the vector-field self-energy explicitly finite. Furthermore, as at the one-loop level the vector-field self-energy involves only the electron propagator, the result turns out to be identical to that computed in the context of the 2 + 1D QED at one-loop order, which naturally implies the conservation of the current ($p_0 \Pi^{0\nu} + c p_i \Pi^{i\nu} = 0$).

Let us now illustrate the effects of quantum corrections on the vector-field propagator $\Delta_{\mu\nu}^F(p)$. Initially, we consider the static potential of interaction between charged particles when using the free propagator Eq. (3.3). In this case, the static potential of interaction $V_{\text{IL}}(r)$ becomes

$$V_{\text{IL}}(r) = e^2 \int \frac{d^2 \mathbf{p}}{(2\pi)^2} e^{-i\mathbf{p}\cdot\mathbf{r}} \Delta_{00}^F(p_0 = 0, \mathbf{p}), \quad (3.24)$$

or, considering $c = 1$ and Eq. (3.3), the tree-level potential becomes

$$V_{\text{bare}}(r) = -\frac{e^2}{4\pi} \int_0^\infty d|\mathbf{p}| \frac{|\mathbf{p}| J_0(|\mathbf{p}|r)}{\sqrt{\mathbf{p}^2 + m^2}} = -\frac{e^2}{4\pi} \frac{e^{-mr}}{r}, \quad (3.25)$$

with $J_0(pr)$ the Bessel function of the first kind, $r = |\mathbf{r}|$, and $V_{\text{bare}}(r)$ representing the Yukawa potential as expected due to the mass in the (3 + 1)D vector field.

The corrected mediating field propagator $\Delta_{F\mu\nu}^{-1}(p)$ in Eq. (3.24) can be found by substituting Eq. (3.19) in the Schwinger-Dyson equation, i.e.,

$$\Delta_{F\mu\nu}^{-1}(p) = \Delta_{\mu\nu}^{-1}(p) - \Pi_{\mu\nu}(p), \quad (3.26)$$

and using the above form for the one-loop corrected vector-field propagator in place of the free propagator in Eq. (3.24).

We now obtain

$$V_{\text{IL}}(r) = e^2 \int \frac{d^2 p}{(2\pi)^2} \frac{e^{-i\mathbf{p}\cdot\mathbf{r}}}{2\sqrt{\mathbf{p}^2 + m^2} - \Pi_{00}(p_0 = 0, \mathbf{p})}. \quad (3.27)$$

From the equation above, we can approximate the effect of the polarization tensor, given by Eq. (3.20), for small ($p \ll M$) and large ($p \gg M$) momentum and obtain the interaction potential for each case to compare it with Ref. [16]. For small momentum within the loop (large distance), it is

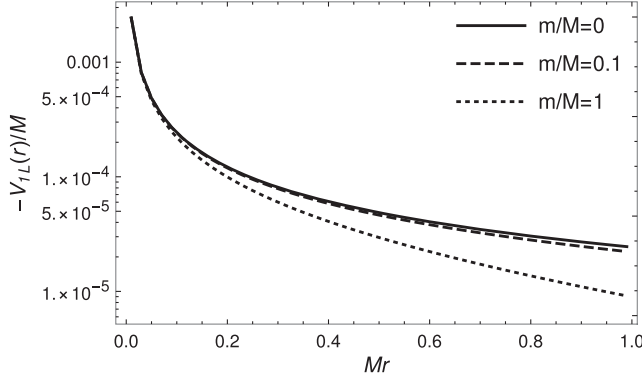


FIG. 5. Interaction potential as a function of the distance [Eq. (3.27)]. The solid line is the same obtained analytically for $m = 0$ in Ref. [16], and the interaction range is significantly shortened as the vector-field mass m grows.

$$V_{1L}(r)|_{p \ll M} \simeq -\frac{e^2}{2\pi} \int_0^\infty d|\mathbf{p}| \frac{|\mathbf{p}| J_0(|\mathbf{p}|r)}{2\sqrt{\mathbf{p}^2 + m^2} + \frac{e^2}{6\pi M} \mathbf{p}^2} \quad (3.28)$$

and can be seen in Fig. 5, while for large loop momentum (short distance) the potential is

$$V_{1L}(r)|_{p \gg M} \simeq -\frac{e^2}{2\pi} \int_0^\infty d|\mathbf{p}| \frac{|\mathbf{p}| J_0(|\mathbf{p}|r)}{2\sqrt{\mathbf{p}^2 + m^2} + \frac{e^2}{8} |\mathbf{p}|}, \quad (3.29)$$

where we consider $v_F = c/300$ and generate Fig. 5.

Notice that, in the limit where m goes to zero, Eq. (3.28) gives the Keldysh potential [46]

$$V_{1L}(r)|_{p \ll M} \simeq -\frac{e^2}{8r_0} \left[H_0\left(\frac{r}{r_0}\right) - Y_0\left(\frac{r}{r_0}\right) \right], \quad (3.30)$$

with a screening length $r_0 = e^2/(12\pi M)$, used to describe the excitonic spectrum of TMDs [47,48], whereas Eq. (3.29) yields a screened Coulomb potential:

$$V_{1L}(r)|_{p \gg M} \simeq -\frac{e^2}{2\pi} \frac{1}{(2 + e^2/8)} \frac{1}{r}. \quad (3.31)$$

This screening effect on the Coulomb potential leads to an effective dielectric constant. This effect has been used to compare experimental data on the renormalization of the Fermi velocity of electrons in graphene [49].

C. Vertex correction and the g factor

To have a complete one-loop analysis of relevant quantities, we also compute next the one-loop interaction vertex radiative contribution Γ_{1L}^ν as shown in Fig. 6.

Explicitly, Γ_{1L}^ν is given by

$$\Gamma_{1L}^\nu = \int \frac{d^D k}{(2\pi)^D} \Gamma^\alpha S_F(k + p') \Gamma^\nu S_F(k + p) \Gamma^\beta \Delta_{\alpha\beta}(k), \quad (3.32)$$

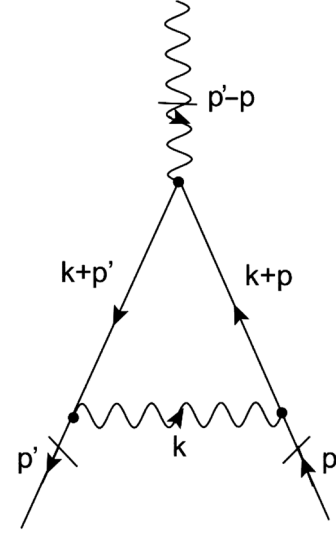


FIG. 6. Feynman diagram for the one-loop correction to the interaction vertex.

but, in order to consider the Gordon decomposition, we include the external lines and identify the terms that have an impact on the g factor with the structure (for further detail, refer to the Appendix)

$$M_{gy}^i = ie\beta\bar{u}(p') \left(\frac{i}{2Mc^2} F_2 v_F \sigma^{i\nu} q_\nu \right) u(p), \quad (3.33)$$

where F_2 generalizes the form factor related to the g factor in Ref. [32] to account for the contribution of the vector-field mass m :

$$F_2 = -\frac{\alpha^* \beta^3}{2\pi} R, \quad (3.34)$$

with $\alpha^* = e^2/4\pi v_F$ the effective fine-structure constant and $R = R(\beta, m/M)$ an effective parametric factor that depends on the mass ratio given by

$$R = \int_0^1 \int_0^{1-x} \frac{2(1+2\beta^2)(x+y) + \beta^2(x+y)^2}{\frac{m^2}{M^2}(1-x-y)\mathcal{D}^2 - (x+y)^2\mathcal{D}} \frac{dydx}{\sqrt{1-x-y}}. \quad (3.35)$$

A few predictions emerge from the result in Eq. (3.34) when looking at some of the limits achievable through the tweak of mass parameters.

When the vector field is heavy with respect to the electron mass, $m \gg M$, the parametric integral no longer depends on the mass ratio, and the parametric factor R

$$R|_{m \gg M} \simeq \frac{M^2}{m^2} \int_0^1 dx \int_0^{1-x} \frac{dy(x+y)}{(1-x-y)^{3/2}} \times \frac{2+4\beta^2+\beta^2(x+y)}{[(1-\beta^2)(x+y)-1]^2} \quad (3.36)$$

implies that $F_2 = 0$; i.e., the g -factor correction vanishes.

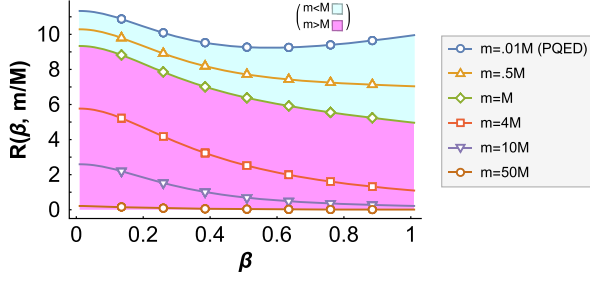


FIG. 7. Dependence of R on the ratio m/M of the three-dimensional vector-field mass to the electron mass. For $(m/M)=0$, the PQED results are retrieved, and for $(m/M) \gg 1$ the g -factor correction is vanishingly small. The solid blue line (obtained near the limit of a nonmassive gauge field) is related to PQED and gives the approximate values of R to correct the g factor obtained in Ref. [32].

The second relevant limit happens when m goes to zero in the original unprojected model, which after the projection reproduces the usual PQED behavior, i.e.,

$$\lim_{m \rightarrow 0} F_2 = F_2^{\text{PQED}}. \quad (3.37)$$

As a consistency check, we take the limit of Eq. (3.35) when $(m/M) \rightarrow 0$ to obtain

$$R = \int_0^1 dx \int_0^{1-x} \frac{dy}{\sqrt{1-x-y}} \left[\frac{2 + 4\beta^2 + \beta^2(x+y)}{(x+y)[1 - (1-\beta^2)(x+y)]} + \frac{\beta_F^2}{[\beta_F^2(x+y) + 1 - x - y]^2} \right] \quad (3.38)$$

and draw an immediate comparison to the parametric integral in Ref. [32], which obtains a similar integration structure but with an incomplete overall numerator. Hence, our model extends the projection to the massive case but also corrects the nonmassive g -factor result for graphene found previously in Ref. [32].

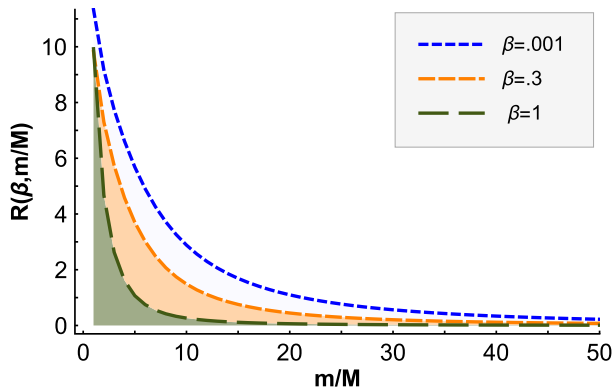


FIG. 8. Dependence of R on the ratio (m/M) for some values of β obtained numerically. We notice that the vector-field mass suppresses the result of the integral (and, consequently, of the g factor) for all values of β , but does it faster for ultrarelativistic systems ($v_F \approx c$).

Although we could not find an analytical solution for the integral in Eq. (3.35), some numerical solutions for R are shown in Fig. 7 for different mass ratios (m/M) . These numerical values of R , when substituted into Eq. (3.34), allow us to verify how small changes in β affect the g factor in each case.

To show that the g factor associated with the system is going to decrease faster with the mass when v_F gets closer to c , we plot in Fig. 8 the numerical values of R for a few different values of β , but now as a function of the mass ratio (m/M) .

IV. CONCLUSIONS

In this work, we have provided a generalization of the dimensional reduction, developed in Ref. [23], for the case of a $(2+1)D$ massive vector field. By doing so, we have obtained an effective planar model that retains the fundamental physical properties of the Proca electrodynamics, which is taken as an effective model for describing massive (via the Anderson-Higgs-Meissner mechanism) photons in a material. We have then evaluated the one-loop radiative corrections for the electron and vector-field self-energies for this model.

We observed that the divergent part of the electron self-energy is exactly identical to the one obtained in the context of the PQED (massless) model. Therefore, from the renormalization group perspective, the renormalization of the Fermi velocity does not depend on the mass of the vector field and, consequently, is the same obtained for the PQED model [12,45], which is similar to the nonlocal Chern-Simons term coupled to PQED obtained from dual transformations in Ref. [34], which also does not affect the Fermi velocity renormalization [50]. The renormalized mass for the electron, on the other hand, is seen to increase with the vector-field mass.

From the vector self-energy, we calculate the polarization tensor in the respective regimes of small and large energies with respect to the fermion mass to estimate the screening effect on the potential for the interaction between fermions; in the massless vectorial gauge field case, these regimes lead to the Keldysh and Coulomb (with screening) potentials, respectively. Here, we have generalized these two potentials to the large-mass vector-field case and identified that they have no bound state for neither the small- nor the large-momentum approximation, just like the regular Proca model with large photon mass [51].

A particular interest in the kind of model studied here is that, from the vertex diagram, it is possible to predict the g factor for the so-called Dirac systems, which exhibit quasirelativistic dynamics, with massless (e.g., graphene) or massive (e.g., silicene and TMDs) electrons moving with the Fermi velocity [32]. In this context, we have found that the parametric integral in the vertex correction form factor—and, thus, this theory's predicted g factor—decreases with both the value of β and the ratio (m/M) , effectively

switching the magnetic coupling off of the system for very large values of m and corrected the result in Ref. [32] for the limit of massless photons ($m \rightarrow 0$).

This work contributes to the proper description of planar effective models, which are known to be intrinsically related to condensed-matter physical systems that can operate as QFT laboratories, such as Dirac materials [52], by investigating the effects of attributing a mass to the interaction field.

ACKNOWLEDGMENTS

R. F. O. is partially supported by Coordenação de Aperfeiçoamento de Pessoal de Nível Superior—Brasil (CAPES), finance code 001, and by CAPES/NUFFIC, finance code 0112; V. S. A. and L. O. N. are partially supported by research grants from Conselho Nacional de Desenvolvimento Científico e Tecnológico (CNPq) and by CAPES/NUFFIC, finance code 0112; V. S. A. acknowledges the Institute for Theoretical Physics of Utrecht University for the kind hospitality and M. Gomes for very fruitful discussions; E. C. M. is partially supported by both CNPq and Fundação Carlos Chagas Filho de Amparo à Pesquisa do Estado do Rio de Janeiro (FAPERJ). R. O. R. is partially supported by research grants from CNPq, Grant No. 307286/2021-5, from Fundação Carlos Chagas Filho de Amparo à Pesquisa do Estado do Rio de Janeiro (FAPERJ), Grant No. E-26/201.297/2021, and by CAPES finance code 1. The authors are also grateful to M. C. Lima, G. C. Magalhães, and M. A. Caracanhas for interesting discussions about the model.

APPENDIX: VERTEX CORRECTION

To shed some light on the g -factor corrections that we have brought up in Sec. III C, we display a part of the calculations of the corrected vertex highlighting the steps that differ from the usual QED. The subtlety on the calculation that appears for the model discussed here comes from the fact that it is anisotropic and has a different photonlike propagator (the planar projection of a massive vector field).

We will analyze the quantity $M^i = \bar{u}(p')\Gamma^i u(p)$, which relates to the two external fermion lines $\bar{u}(p')$ and $u(p)$ in the spatial component of the vertex diagram (because the temporal part of it does not affect the g factor), such that we can use the Dirac equations to simplify the calculations further.

Starting from the vertex structure in Sec. III C,

$$\Gamma_{\text{IL}}^\nu = \int \frac{d^D k}{(2\pi)^D} \Gamma^\alpha S_F(k+p') \underbrace{\Gamma^\nu S_F(k+p)}_{\rho^\nu} \Gamma^\beta \Delta_{\alpha\beta}(k), \quad (\text{A1})$$

we define an auxiliary variable ρ^ν and expand the indices α and β to get

$$\Gamma_{\text{IL}}^\nu = \int \frac{d^D k}{(2\pi)^D} [\Gamma^0 \rho^\nu \Gamma^0 \Delta_{00}(k) + \Gamma^l \rho^\nu \Gamma^n \Delta_{ln}(k)]. \quad (\text{A2})$$

In Eq. (A2), the nondiagonal terms of the vector-field propagator were dropped, because the metrics inside them vanish. Explicitly substituting the Feynman rules given in Sec. III, we find

$$\begin{aligned} \Gamma_{\text{IL}}^\nu = & -\frac{ie^2 c}{2} \mu \int \frac{d^D k}{(2\pi)^D} \left[\frac{1}{\sqrt{k_0^2 - c^2 \mathbf{k}^2 - m^2 c^4}} \right] \\ & \times \left\{ \gamma^0 \left(\frac{\gamma^0(k+p')_0 + v_F \gamma^i(k+p')_i + M c^2}{(k+p')_0^2 - v_F^2(\mathbf{k}+\mathbf{p}')^2 - M^2 c^4} \right) \Gamma^\nu \left(\frac{\gamma^0(k+p)_0 + v_F \gamma^i(k+p)_i + M c^2}{(k+p)_0^2 - v_F^2(\mathbf{k}+\mathbf{p})^2 - M^2 c^4} \right) \gamma^0 \right. \\ & \left. + \beta^2 \gamma^l \left(\frac{\gamma^0(k+p')_0 + v_F \gamma^i(k+p')_i + M c^2}{(k+p')_0^2 - v_F^2(\mathbf{k}+\mathbf{p}')^2 - M^2 c^4} \right) \Gamma^\nu \left(\frac{\gamma^0(k+p)_0 + v_F \gamma^i(k+p)_i + M c^2}{(k+p)_0^2 - v_F^2(\mathbf{k}+\mathbf{p})^2 - M^2 c^4} \right) \gamma^n \eta_{ln} \right\}. \quad (\text{A3}) \end{aligned}$$

To handle this unusual propagator, which contains a square root and a mass term, we apply a slightly modified Feynman parametrization:

$$\frac{1}{abd^{1/2}} = \frac{3}{4} \int_0^1 dx \int_0^{1-x} dy \frac{(1-x-y)^{-1/2}}{[ax + by + d(1-x-y)]^{5/2}} \quad (\text{A4})$$

on the denominator of each term in Eq. (A3). Assuming

$$\begin{aligned} a &= (k+p')_0^2 - v_F^2(\mathbf{k}+\mathbf{p}')^2 - M^2 c^4, \\ b &= (k+p)_0^2 - v_F^2(\mathbf{k}+\mathbf{p})^2 - M^2 c^4, \quad d = 3k_0^2 - c^2, \end{aligned} \quad (\text{A5})$$

we find that the denominator of Eq. (A3) is given by

$$\begin{aligned} \frac{1}{abc^{1/2}} = & \frac{3}{4} \int_0^1 dx \int_0^{1-x} \frac{dy}{\sqrt{1-x-y}} \{ k_0^2(1+x+y) \\ & + [2k_0 p'_0 + p_0'^2]x - m^2 c^4(1-x-y) \\ & + [2k_0 p_0 + p_0^2 - v_F^2(k+p)^2 \\ & - M^2 c^4]y - c^2 \mathbf{k}^2 \}^{-5/2}. \quad (\text{A6}) \end{aligned}$$

Now, we complete the k_0 square, make a shift $k_0 \rightarrow k_0 - \omega_0$ (with $\omega_0 = xp'_0 + yp_0$) on it, and solve the integration over k_0 as done in standard anisotropic procedures (at this point, we also drop the odd terms in k_0).

Then, we follow essentially the same steps for \mathbf{k} but using the shift $\mathbf{k} \rightarrow \mathbf{k} - \omega\beta^2/\mathcal{D}^2$, with $\mathcal{D} = [(1 - \beta^2)(x + y) - 1]$ and $\omega = xp' + yp$. Finally, we perform the integration over \mathbf{k} using dimensional regularization [42] to obtain Eq. (A8), namely,

$$\Gamma_{\text{IL}}^i = \int_0^1 dx \int_0^{1-x} \frac{dy}{6\pi^2} \left[\frac{N_3}{\mathcal{K}} \right] \frac{Mp^i v_F^2}{\sqrt{1-x-y}}, \quad (\text{A7})$$

where, for convenience, we defined the numerator result for the integration in \mathbf{k} as

$$N_3 = \frac{2(1-x-y)\gamma^j \omega_j p_i v_F^2}{\mathcal{D}} - \frac{[\omega_i - 2(x+y)^2 p_i] \beta^4}{\mathcal{D}^2},$$

$$\mathcal{D} = [(1 - \beta^2)(x + y) - 1],$$

and its denominator as

$$\mathcal{K} = \mathcal{D}^2 (M^2 c^4 - m^2 c^4 - \omega_0^2) c^2 + [v_F^2 (p' - p)_i^2 + p_0^2] xy$$

$$+ [(x + y)(1 - x - y) c^2] (p' + p)_\mu^2 + p_0^2 y^2.$$

When represented according to the flux choices in Fig. 6 and after applying a parametrization detailed above, the diagram is written in its parametrized form as

$$M^i = \bar{u}(p') \left(\int_0^1 dx \int_0^{1-x} \frac{dy}{6\pi^2} \frac{Mp^i v_F^2}{\sqrt{1-x-y}} \frac{N_3}{\mathcal{K}} \right) u(p), \quad (\text{A8})$$

with

$$N_3 = \frac{2(1-x-y)\gamma^j \omega_j p_i v_F^2}{[(1 - \beta^2)(x + y) - 1]} - \frac{[\omega_i - 2(x+y)^2 p_i] \beta^4}{[(1 - \beta^2)(x + y) - 1]^2}, \quad (\text{A9})$$

$$\mathcal{K} = [(1 - \beta^2)(x + y) - 1]^2 (M^2 c^4 - m^2 c^4 - \omega_0^2) c^2$$

$$+ [v_F^2 (p' - p)_i^2 + p_0^2] xy$$

$$+ [(x + y)(1 - x - y) c^2] (p' + p)_\mu^2 + p_0^2 y^2, \quad (\text{A10})$$

where $\omega_0 = xp'_0 + yp_0$ and $\omega_i = xp'_i + yp_i$.

Then, using the (Gordon) decomposition identity

$$\bar{u}(p') \gamma^\mu u(p) = \bar{u}(p') \left[\frac{(p' + p)^\mu}{2Mc^2} + i\sigma^{\nu\mu} \frac{q_\nu}{2Mc^2} \right] u(p)$$

[where $\bar{u}(p')$ and $u(p)$ are spinorial solutions to the Dirac equations, $q_\nu = (p' - p)_\nu$ is the transferred momentum, and $\sigma_{\nu\mu} = (i/2)[\gamma_\nu, \gamma_\mu]$], we determine the M^i relevant terms to the g factor. In other words, we expand Eq. (A8), selecting only the terms proportional to $\sigma^{i\alpha}$ and leaving aside the terms that would have a $(p' + p)^\mu$ to define

$$M_{gy}^i = \bar{u}(p') \left\{ \int_0^1 dx \int_0^{1-x} \frac{dy}{6\pi^2} \frac{Mv_F \sigma^{i\alpha} (p' - p)_\alpha \beta^2}{\mathcal{K} \sqrt{1-x-y}} \right.$$

$$\left. \times \left[\frac{2(1-2\beta^2)(x+y)^2 - 2(x+y)}{[(1 - \beta^2)(x + y) - 1]^2} \right] \right\} u(p), \quad (\text{A11})$$

where the subscribed “gy” index was used to identify that we are accounting for only the $\sigma^{i\alpha}$ proportional parcels.

To extract the g factor, however, a few extra conditions are also necessary, such as the low-energy approximation ($q^2 \rightarrow 0$) and the mass-shell condition (which for small-energy values reads as $v_F \gamma^j p_j \cong Mc^2$) [32,42]. After taking the above conditions, we conveniently define a variable

$$\mathcal{K}' = \{ [(x + y)^2 - x - y] v_F^2 - [(1 - x - y)^2] c^2 \} m^2 c^4$$

$$+ 2\{ [(x + y)^2 - x - y] c^2 - 2(x + y)^2 v_F^2 \} M^2 c^4, \quad (\text{A12})$$

so that the g -factor relevant parcel of the vertex correction M_{gy}^i is reduced to

$$M_{gy}^i = \bar{u}(p') \left\{ \frac{1}{6\pi^2} \int_0^1 dx \int_0^{1-x} dy \frac{M^2 c^2 \sigma^{i\alpha} q_\alpha v_F^3}{\mathcal{K}' \sqrt{1-x-y}} \right.$$

$$\left. \times [2(x + y)\mathcal{D} - (x + y)^2 v_F^2] \right\} u(p). \quad (\text{A13})$$

From this structure, we identify the form factor F_2 detailed in Sec. III C.

-
- [1] T. Ando, Y. Matsumoto, and Y. Uemura, Theory of Hall effect in a two-dimensional electron system, *J. Phys. Soc. Jpn.* **39**, 279 (1975).
 [2] D. C. Tsui, H. L. Stormer, and A. C. Gossard, Two-Dimensional Magnetotransport in the Extreme Quantum Limit, *Phys. Rev. Lett.* **48**, 1559 (1982).

- [3] R. B. Laughlin, Anomalous Quantum Hall Effect: An Incompressible Quantum Fluid with Fractionally Charged Excitations, *Phys. Rev. Lett.* **50**, 1395 (1983).
 [4] C. C. Chamon and E. Fradkin, Distinct universal conductances in tunneling to quantum Hall states: The role of contacts, *Phys. Rev. B* **56**, 2012 (1997).

- [5] O. Heinonen, *Composite Fermions: A Unified View of the Quantum Hall Regime* (World Scientific, Singapore, 1998), and articles therein.
- [6] E. V. Gorbar, V. P. Gusynin, V. A. Miransky, and I. A. Shovkovy, Coulomb interaction and magnetic catalysis in the quantum Hall effect in graphene, *Phys. Scr. T* **146**, 014018 (2012).
- [7] I. F. Herbut, Interactions and Phase Transitions on Graphene's Honeycomb Lattice, *Phys. Rev. Lett.* **97**, 146401 (2006).
- [8] V. P. Gusynin, V. A. Miransky, S. G. Sharapov, and I. A. Shovkovy, Excitonic gap, phase transition, and quantum Hall effect in graphene, *Phys. Rev. B* **74**, 195429 (2006).
- [9] I. F. Herbut, V. Juricic, and O. Vafek, Coulomb Interaction, Ripples, and the Minimal Conductivity of Graphene, *Phys. Rev. Lett.* **100**, 046403 (2008).
- [10] V. Juricic, I. F. Herbut, and G. W. Semenoff, Coulomb interaction at the metal-insulator critical point in graphene, *Phys. Rev. B* **80**, 081405 (2009).
- [11] M. A. H. Vozmediano, M. I. Katsnelson, and F. Guinea, Gauge fields in graphene, *Phys. Rep.* **496**, 109 (2010).
- [12] M. A. H. Vozmediano and F. Guinea, Effect of Coulomb interactions on the physical observables of graphene, *Phys. Scr. T* **146**, 014015 (2011).
- [13] E. C. Marino, L. O. Nascimento, V. S. Alves, and C. M. Smith, Interaction Induced Quantum Valley Hall Effect in Graphene, *Phys. Rev. X* **5**, 011040 (2015).
- [14] N. Menezes, V. S. Alves, and C. M. Smith, The influence of a weak magnetic field in the Renormalization-Group functions of $(2 + 1)$ -dimensional Dirac systems, *Eur. Phys. J. B* **89**, 271 (2016).
- [15] W. Choi, N. Choudhary, G. H. Han, J. Park, D. Akinwande, and Y. H. Lee, Recent development of two-dimensional transition metal dichalcogenides and their applications, *Mater. Today* **20**, 116 (2017).
- [16] E. C. Marino, L. O. Nascimento, V. S. Alves, N. Menezes, and C. M. Smith, Quantum-electrodynamical approach to the exciton spectrum in transition-metal dichalcogenides, *2D Mater.* **5**, 041006 (2018).
- [17] A. J. Chaves, R. M. Ribeiro, T. Frederico, and N. M. R. Peres, Excitonic effects in the optical properties of 2D materials: an equation of motion approach, *2D Mater.* **4**, 025086 (2017).
- [18] Z. Tesanovic, L. Xing, L. Bulaevskii, Q. Li, and M. Suenaga, Critical Fluctuations in the Thermodynamics of Quasi-Two-Dimensional Type-II Superconductors, *Phys. Rev. Lett.* **69**, 3563 (1992).
- [19] S.-C. Zhang, SO(5) quantum nonlinear sigma model theory of the high T_c superconductivity, *Science* **275**, 1089 (1997).
- [20] M. Franz, Z. Tesanovic, and O. Vafek, QED₃ theory of pairing pseudogap in cuprates: From d-wave superconductor to antiferromagnet via an algebraic Fermi liquid, *Phys. Rev. B* **66**, 054535 (2002).
- [21] S. A. Kivelson, I. P. Bindloss, E. Fradkin, V. Oganesyan, J. M. Tranquada, A. Kapitulnik, and C. Howald, How to detect fluctuating stripes in the high-temperature superconductors, *Rev. Mod. Phys.* **75**, 1201 (2003).
- [22] E. C. Marino, D. Niemeyer, V. S. Alves, T. Hansson, and S. Moroz, Screening and topological order in thin superconducting films, *New J. Phys.* **20**, 083049 (2018).
- [23] E. C. Marino, Quantum electrodynamics of particles on a plane and the Chern-Simons theory, *Nucl. Phys.* **B408**, 551 (1993).
- [24] E. V. Gorbar, V. P. Gusynin, and V. A. Miransky, Dynamical chiral symmetry breaking on a brane in reduced QED, *Phys. Rev. D* **64**, 105028 (2001).
- [25] S. Teber, Electromagnetic current correlations in reduced quantum electrodynamics, *Phys. Rev. D* **86**, 025005 (2012).
- [26] A. V. Kotikov and S. Teber, Two-loop Fermion self-energy in reduced quantum electrodynamics and application to the ultrarelativistic limit of graphene, *Phys. Rev. D* **89**, 065038 (2014).
- [27] E. C. Marino, L. O. Nascimento, V. S. Alves, and C. M. Smith, Unitarity of theories containing fractional powers of the d'Alembertian operator, *Phys. Rev. D* **90**, 105003 (2014).
- [28] R. L. P. G. do Amaral and E. C. Marino, Canonical quantization of theories containing fractional powers of the d'Alembertian operator, *J. Phys. A* **25**, 5183 (1992).
- [29] L. Fernández, V. S. Alves, L. O. Nascimento, F. Peña, M. Gomes, and E. C. Marino, Renormalization of the band gap in 2D materials through the competition between electromagnetic and four-fermion interactions, *Phys. Rev. D* **102**, 016020 (2020).
- [30] J. D. Silva, A. N. Braga, W. P. Pires, V. S. Alves, D. T. Alves, and E. C. Marino, Inhibition of the Fermi velocity renormalization in a graphene sheet by the presence of a conducting plate, *Nucl. Phys.* **B920**, 221 (2017).
- [31] W. P. Pires, J. D. Silva, A. N. Braga, V. S. Alves, D. T. Alves, and E. C. Marino, Cavity effects on the Fermi velocity renormalization in a graphene sheet, *Nucl. Phys.* **B932**, 529 (2018).
- [32] N. Menezes, V. S. Alves, E. C. Marino, L. Nascimento, L. O. Nascimento, and C. M. Smith, Spin g-factor due to electronic interactions in graphene, *Phys. Rev. B* **95**, 245138 (2016).
- [33] V. S. Alves, W. S. Elias, L. O. Nascimento, V. Juričić, and F. Peña, Chiral symmetry breaking in the pseudo-quantum electrodynamics, *Phys. Rev. D* **87**, 125002 (2013).
- [34] V. S. Alves, E. C. Marino, L. O. Nascimento, J. F. Medeiros Neto, R. F. Ozela, and R. O. Ramos, Bounded particle interactions driven by a nonlocal dual Chern-Simons model, *Phys. Lett. B* **797**, 134860 (2019).
- [35] P. R. S. Gomes and M. Gomes, Higher spatial derivative field theories, *Phys. Rev. D* **85**, 089909 (2012).
- [36] D. Anselmi and M. Halat, Renormalization of Lorentz violating theories, *Phys. Rev. D* **76**, 125011 (2007).
- [37] D. Anselmi, Weighted power counting and Lorentz violating gauge theories. I: General properties, *Ann. Phys. (Amsterdam)* **324**, 874 (2009).
- [38] M. Visser, Lorentz symmetry breaking as a quantum field theory regulator, *Phys. Rev. D* **80**, 025011 (2009).
- [39] P. Hořava, Quantum gravity at a Lifshitz point, *Phys. Rev. D* **79**, 084008 (2009).
- [40] D. Blas, O. Pujolas, and S. Sibiryakov, Consistent Extension of Hořava Gravity, *Phys. Rev. Lett.* **104**, 181302 (2010).
- [41] V. S. Alves, T. Macrì, G. C. Magalhães, E. C. Marino, and L. O. Nascimento, Two-dimensional Yukawa interactions from nonlocal Proca quantum electrodynamics, *Phys. Rev. D* **97**, 096003 (2018).

- [42] M.E. Peskin and D.V. Schroeder, *An Introduction to Quantum Field Theory* (Perseus, New York, 1995); M.O.C. Gomes, *Teoria Quântica dos Campos* (Edusp, 2002) (in Portuguese).
- [43] C. Bollini and J.J. Giambiagi, Dimensional renormalization: The number of dimensions as a regularizing parameter, *Il Nuovo Cimento B*, **12**, 20 (1972).
- [44] G. 't Hooft and M. Veltman, Regularization and renormalization of gauge fields, *Nucl. Phys.* **B44**, 189 (1972).
- [45] E.C. Marino, *Quantum Field Theory Approach to Condensed Matter Physics* (Cambridge University Press, Cambridge, England, 2017).
- [46] L.V. Keldysh, Coulomb interaction in thin semiconductor and semimetal films, *J. Exp. Theor. Phys. Lett.* **29**, 658 (1979).
- [47] A.J. Chaves, R.M. Ribeiro, T. Frederico, and N.M.R. Peres, Excitonic effects in the optical properties of 2D materials: An equation of motion approach, *2D Mater.* **4**, 025086 (2017).
- [48] A. Chernikov, T. c. Berkelbach, H. M. Hill, A. Rigosi, Y. Li, O. B. Aslan, D. R. Reichman, M. S. Hybertsen, and T. F. Heinz, Exciton Binding Energy and Nonhydrogenic Rydberg Series in Monolayer WS₂, *Phys. Rev. Lett.* **113**, 076802 (2014).
- [49] D. C. Elias, R. V. Gorbachev, A. S. Mayorov, S. V. Morozov, A. A. Zhukov, P. Blake, L. A. Ponomarenko, I. V. Grigorieva, K. S. Novoselov, F. Guinea, and A. K. Geim, Dirac cones reshaped by interaction effects in suspended graphene, *Nat. Phys.* **7**, 701 (2011).
- [50] G. C. Magalhães, V. S. Alves, L. O. Nascimento, and E. C. Marino, Bosonization, mass generation, and the pseudo-Chern-Simons action, *Phys. Rev. D* **103**, 116022 (2021).
- [51] Y. Li, X. Luo, and H. Kröger, Bound states and critical behavior of the Yukawa potential, *Sci. China Ser. G* **49**, 60 (2006).
- [52] A. H. Castro Neto, F. Guinea, N.M.R. Peres, K. S. Novoselov, and A. K. Geim, The electronic properties of graphene, *Rev. Mod. Phys.* **81**, 109 (2009).